Journal of
Materials Chemistry B

Accepted Manuscript

This is an *Accepted Manuscript*, which has been through the RSC Publishing peer review process and has been accepted for publication.

Accepted Manuscripts are published online shortly after acceptance, which is prior to technical editing, formatting and proof reading. This free service from RSC Publishing allows authors to make their results available to the community, in citable form, before publication of the edited article. This *Accepted Manuscript* will be replaced by the edited and formatted *Advance Article* as soon as this is available.

To cite this manuscript please use its permanent Digital Object Identifier (DOI®), which is identical for all formats of publication.

More information about *Accepted Manuscripts* can be found in the **Information for Authors**.

Please note that technical editing may introduce minor changes to the text and/or graphics contained in the manuscript submitted by the author(s) which may alter content, and that the standard **Terms & Conditions** and the **ethical guidelines** that apply to the journal are still applicable. In no event shall the RSC be held responsible for any errors or omissions in these *Accepted Manuscript* manuscripts or any consequences arising from the use of any information contained in them.

The influence of fluorocarbon chain and phosphorylcholine on the improvement of hemocompatibility: a comparative study in polyurethanes

Dongsheng Tan, Zhen Li, Xuelin Yao, Chunlan Xiang, Hong Tan*, Qiang Fu*

College of Polymer Science and Engineering,

State Key Laboratory of Polymer Materials Engineering,

Sichuan University, Chengdu 610065, China

Abstract

To study the influence of fluorinated surface and biomimetic surface on the improvement of blood compatibility of polymers, three monomers containing fluorinated tail and/or phosphorylcholine group were designed and synthesized, and then were introduced to polyurethanes based on 4,4'-diphenylmethane diisocyanate (MDI), poly(tetramethylene glycol) (PTMG) and 1,4-butanediol (BDO) via end-capping. The bulk and surface characterization of polyurethanes was investigated by dynamic mechanical analysis (DMA), Fourier transform infrared spectroscopy (FTIR), X-ray photoelectron spectroscopic analysis (XPS), atomic force microscope (AFM), and water contact angle measurements. The results indicate that the fluorocarbon chains can drive the phosphorylcholine groups to enrich on the surface of polyurethane, and the two components show spontaneous arrangement to adapt to environment when contacting with water. The preliminary evaluation of hemocompatibility was carried out via fibrinogen adsorption and platelet adhesion. The fluorocarbon chains and phosphorylcholine groups showed synergistic effect on the improvement of hemocompatibility.

Key words: fluorocarbon chain, phosphorylcholine, polyurethane, hemocompatibility, blood compatibility

* Corresponding authors, Tel.: +86-28-85460961; Fax: +86-28-85405402.
Email: qiangfu@scu.edu.cn (Q. Fu); hongtan@scu.edu.cn (H. Tan).

1. Introduction

Various polymers used in biomaterial field need to be modified to improve their biocompatibility, mechanical properties, hydrolysis resistance properties, or other functionalities. In blood contacting materials, most research strategies consist in modulating the interface by modifying the synthetic graft surface properties, with the aim to improve their hemocompatibility[1-6]. For instance, polyurethanes are now widely used in biomedical apparatus and instruments because of their relatively good antithrombogenicity, excellent compliance, and beneficial physical/mechanical properties, while the compatibility of PU with blood is not satisfactory enough for making small-diameter vascular prostheses in vivo applications[3, 7], and surface fluorination and surface biomimetic design are two efficient ways among the modification methods for improving hemocompatibility.

It is well-known that fluorocarbon chains exhibit unique characteristics, such as low surface energy, oxidative stability, and good water and oil repulsion[4, 8]. As a result, a large number of fluorinated polymers have been found to be relatively hemocompatible. Xie et al. applied a fluorinated alcohol to end-cap the poly(carbonate urethane)s, the fluorinated poly(carbonate urethane)s revealed an unique bilayered surface structure, which effectively improved the biostability and antiplatelet adhesion performance of this kind of polyurethanes[9]. Fluorocarbon chains have also been introduced to the chain extender (in hard segment) or the soft segment of polyurethanes[10, 11]. The fluorocarbon chains could usually enhance the phase separation and migrate to the top surface, resulting in polyurethane samples exhibiting low surface energies and good blood compatibility. In fact, *in vitro* platelet test has exhibited that the platelet compatibility of polyurethanes could be improved when the fluorocarbon oligomers were directly grafted to the surface of polyurethanes[12, 13].

Introducing phospholipid analoges to form biomembrane mimicking polymers is another effective way to improve hemocompatibility by suppressing protein adsorption, platelet adhesion, and platelet activation on the surface of materials[14-17]. It

is known that surface characteristics always play a decisive role in blood compatibility of biomaterials, and the free and bound water on the surface of biomimetic polymers have been proved to play a crucial role in the outstanding biocompatibility[18, 19]. Therefore, the phospholipid moieties should be designed to appear at the interface of polyurethane surfaces to function. For example, Iwasaki et al. prepared the semi-interpenetrating polymer networks (IPNs) by the radical polymerization of diffused 2-methacryloyloxyethyl phosphorylcholine (MPC) in the segmented polyurethane membranes[20]; Lee et al. used the poly (MPC-*co*-*n*-butyl methacrylate) solution to coat on polyurethane surfaces to form phospholipid interface, which showed a qualitative improvement in hemocompatibility during implantation[5].

Both of the fluorocarbon chain and the phosphorylcholine have been demonstrated to effectively improve the blood compatibility of polymers by being introduced on the surfaces. It is unclear, however, which is more effective on the improvement of hemocompatibility, or a synergistic effect can be acted between them when they both appear in the same surface of polymers? Therefore it motivated us to study the influence of fluorocarbon chain and phosphorylcholine on the improvement of blood compatibility in polyurethanes. In the present work, four kinds of polyurethanes, with different chain ends (fluorocarbon chain and/or phosphorylcholine), were synthesized and characterized to explore the mechanism of anticoagulation effect through comparisons.

2. Experimental

2.1. Materials

2-Chloro-1,3,2-dioxaphospholane-2-oxide (COP, 95%) was purchased from Acros Organics. 2,2,3,3,4,4,5,5,6,6,7,7,8,8,8-pentadecafluorooctanoicacid (95%), 5-Amino-1-pentanol (95%), and dibutyltin dilaurate (DBTDL, 95%) were purchased from Aldrich. 4,4'-diphenylmethane diisocyanate (MDI, Aladdin) and 1,4-butanediol (BDO, Aladdin) were used as received. Poly(tetramethylene glycol) (PTMG, Mw = 1000, obtained from Aldrich) was dehydrated at 100 ^{o}C for 4 h under vacuum**.** Other

reagents and solvents were all obtained from Kelong Co. (Chengdu, China) in AR grade and were used as received.

2.2. Instrumentations

^{1}H NMR spectra were recorded on a Varian Unity INOVA (400 MHz) spectrometer, using tetramethylsilane (TMS) as an internal standard, $CDCl_3$ or DMSO-d_6 as solvents. Mass spectra were obtained on a TSQ Quantum Ultra LC/MS/MS system (San Jose, CA, USA), and the electrospray ionization source was run in positive ion mode for all experiments. Gel permeation chromatography (GPC) was performed by Waters-1515 using N, N-dimethylformamide (DMF)/LiBr as eluent. The molecular weights are relative to polymethyl methacrylate (PMMA) standards. The sample concentration was 2-3 mg/mL, and the flow rate was 1.000 mL/min at 40 °C. XPS was carried out on an XSAM-800 electron spectrometer equipped with an Mg-Kα achromatic X-ray source (20 KV, 10 mA). The contents of phosphorus (P) and fluorine (F) were detected by inductive coupled plasma emission spectrometer (ICP-AES, IRIS 1000, Thermo Fisher Scientific) and ion chromatograph (ICS-90, DIONEX), and three samples were tested, respectively. Thermal transition of the PUs was measured by dynamic mechanical analysis (Q800, TA Instruments-Waters LLC). Fourier transform infrared (FTIR) spectroscopy analysis was performed on a Nicolet-6700 spectrophotometer equipped with a Ge prism at an incident angle of 45°. The AFM measurements were performed on an SPA400/SPI3800N (Seiko Instruments Inc.) with a tapping mode of 0.4 – 0.7 amplitude at room temperature. Contact angles of samples were measured using sessile drop method by using a digital optical contact angle meter DSA100 (KRUSS GmbH, Germany) with 3 μL of water at 25 °C and relative humidity of 80%, and six films were tested for each sample.

2.3. Synthetic part

2.3.1. Synthesis of *tert*-butyl 2-(2,2,3,3,4,4,5,5,6,6,7,7,8,8,8-pentadecafluorooctan amido) ethylcarbamate

A solution of 2,2,3,3,4,4,5,5,6,6,7,7,8,8,8-pentadecafluorooctanoicacid (**a**, 10 g, 24.2 mmol) and N-methylmorpholine (2.92 mL, 26.6 mmol) in anhydrous tetrahydrofuran (100 mL) was cooled to –15 ^{o}C, then isobutyl chlorocarbonate (3.17

mL, 5.0 mmol) was added. After the mixture was stirred for 10 min, BDA (**b**, 3.87 g, 24.2 mmol) in 10 mL anhydrous tetrahydrofuran was added dropwise to the reaction. The reaction mixture was stirred for 2 h at room temperature and the solvent was removed using a rotary evaporator. And then the residue was dissolved in ethyl acetate. The solution was washed with dilute HCl, brine, distilled water, dried over $MgSO_4$, filtered under vacuum and evaporated in vacuum to give crude **c**. The crude **c** was purified by silica gel column chromatography using gradient petroleum ether/ethyl acetate to yield 6.8 g of **c** (50.5%, Rf 0.61 in 60% petroleum ether/ethyl acetate).

APCI ms (positive) m/z theoretical 556 g mol^{-1}, observed 579 g mol^{-1};

^{1}H NMR ($CDCl_3$, 400 MHz) δ ppm: 1.44 (s, 9H, -$C(CH_3)_3$), 3.36–3.41 (m, 2H, -CH_2-), 3.45–3.50 (m, 2H, -CH_2-), 4.92 (s, 1H, -NH-), 7.95 (s, 1H, -NH-).

2.3.2. Synthesis of N-(2-aminoethyl)-2,2,3,3,4,4,5,5,6,7,7,8,8,8-tetradecafluorooctan amide

Compound **c** (5.0 g, 9.0 mmol) was dissolved in 50 mL of ethyl acetate, 20 mL of saturated HCl/ethyl acetate were added and the mixture solution was stirred at ambient temperature for 1 h. After evaporation of the solvent, ethyl ether (50 mL × 3) was added to the residue and the precipitated white crude product was collected by filtration. Then, the crude product was dissolved in methanol, and adjusted to pH 10 by addition of 1N $NaHCO_3$. After removal of the methanol under vacuum, the N-(2-aminoethyl)-2,2,3,3,4,4,5,5,6,7,7,8,8,8-tetradecafluorooctanamide (FA) was extracted with ethyl acetate and further washed with brine and distilled water, dehydrated over anhydrous $MgSO_4$, filtered under vacuum and evaporated in vacuum to yield to 3.5 g of FA (85.3%).

APCI ms (positive) m/z theoretical 456 g mol^{-1}, observed 457 g mol^{-1};

^{1}H NMR (DMSO, 400 MHz) δ ppm: 2.89 (t, 2H, -CH_2N-), 3.43 (t, 2H, -NCH_2-), 5.32 (t, 1H, -NH-), 7.85 (br, 2H, -NH_2).

2.3.3. Synthesis of *tert*-butyl 5-hydroxypentylcarbamate.

To a solution of 5-Amino-1-pentanol (**d**, 10.3 g, 0.1 mol) in dichloromethane (150 mL) was added dropwise the solution of Di-tert-butyl dicarbonate (**e**, 21.8 g, 0.1 mol) in dichloromethane (50 mL) with stirring for 30 min and the mixture was allowed to be stirred 24 h at room temperature. Volatile components were evaporated, and the residue was taken up in ethyl acetate and further washed twice with 0.5 M citric acid and once with H_20. After the mixture was dried ($MgSO_4$,) and the solvent evaporated, the residue was evaporated in vacuum to yield an oil (**f**): 17.5 g (86.2%).

APCI ms (positive) m/z theoretical 204 g mol^{-1}, observed 205 g mol^{-1}

^{1}H NMR ($CDCl_3$, 400 MHz) δ ppm: 1.25 (t, 2H, -CH_2OH), 1.44 (s, 9H, -C(CH_3)$_3$), 1.51 (m, 2H, -CH_2-), 1.59 (m, 2H, -CH_2-), 1.65 (s, 1H, -OH), 3.13 (q, 2H, -CH_2NH-), 3.65 (m, 2H, -CH_2-), 4.56 (s, 1H, -NH-).

2.3.4. Synthesis of 5-aminopentyl 2-(trimethylammonio)ethyl phosphate

Compound **f** (10.0 g, 49.0 mmol) and triethylamine (7.5 mL, 53.9 mmol) were dissolved in anhydrous tetrahydrofuran (80 mL). After cooling the solution down to −15 °C, COP (7.0 g, 49.0 mmol) dissolved in anhydrous tetrahydrofuran (10 mL) was added dropwise to the stirred solution under nitrogen. The temperature of the reaction mixture was maintained at −15 °C for 1 h and allowed to slowly warm up to the room temperature. Triethylammonium chloride precipitate was filtered off and washed with anhydrous tetrahydrofuran. The filtrate was evaporated under vacuum to give the residue as a colorless oil. The residue was dissolved in 60 mL dry acetonitrile and transferred to a 100 mL glass pressure bottle. After the pressure bottle was cooled to −18 °C, excessive trimethylamine was rapidly added to the solution. The pressure bottle was then sealed and maintained at 60 °C for 24 h. Subsequently the solution was evaporated under vacuum to produce a viscous liquid, then dissolved in methanol (20 mL), followed by the addition of saturated HCl/ethyl acetate (10 mL). The mixture was stirred for 2 h, concentrated under reduced pressure, washed with diethyl ether several times, dissolved in methanol (20 mL), adjusted the pH to 9 by addition of saturated sodium bicarbonate solution, and filtered. The filtrate was concentrated under reduced pressure and the crude product was purified by flash column

chromatography (reverse phase silica gel, water/methanol = 10/1) to yield APPC as a white solid (10.2 g, 38.1 mmol, 78%).

APCI ms (positive) m/z theoretical 268 g mol^{-1}, observed 269 g mol^{-1};

^{1}H NMR (DMSO, 400 MHz) δ ppm: 1.38 (m, 2H, -CH_2-), 1.51 (m, 2H, -CH_2-), 1.60 (m, 2H, -CH_2-), 2.74 (t, 2H, -C$\underline{H}_2NH_2$), 3.15 (s, 9H, -$N^+(CH_3)_3$), 3.55 (t, 2H, -CH_2N^+), 3.68 (m, 2H, -CH_2O-), 4.05 (s, 2H, -OCH_2-), 8.20 (s, 2H, -NH_2).

^{13}C NMR (D_2O, 200 MHz) δ ppm: 19.5 (-CH_2-), 23.9 (-CH_2-), 26.7 (-CH_2-), 36.9 (-CH_2NH_2), 51.4 (-$N^+(CH_3)_3$), 56.8 (-CH_2N^+), 56.9 (-CH_2O-), 63.5 (-OCH_2-).

2.3.5. Synthesis of polyurethanes

The control polyurethane based on 3/2/1 molar ratio of MDI/PTMG/BDO, and end-capped polyurethanes based on 3/2/0.5/1 molar ratio of MDI/PTMG/BDO/end-capping reagents were prepared by solution polymerization in a suitable solvent with DBTDL catalyst. All polyurethanes were synthesized by similar methods. A representative synthesis of PU-PC (PTMG-MDI-BDO-PC) is described as follows.

In the first reaction step: MDI and 0.5% DBDTL were added to the stirred toluene solution of PTMG under a dry nitrogen atmosphere at 60 °C. The reaction was maintained at 60 °C for 2 h. In the second step, chain extender (BDO) was added to the reaction solution, while the temperature was kept at 70 °C for 1 h. Following this, the APPC dissolved in DMF was added to the mixture and allowed to be stirred at 80 °C for 1 h. The solution was then cooled to room temperature. The polymer was precipitated in methanol/distilled water mixed solvent (vol/vol = 4/1) to remove any residual APPC and the low molecular weight fraction, then dried in an oven for 24 h, and followed by drying at 60 °C under vacuum for 48 h.

The reaction scheme for synthesis of polyurethanes is shown in Scheme 2. Characteristics of the polymer (PU-PC) are summarized here:

FTIR (neat, cm^{-1}): 3297 (NH); 2940, 2856, 2799 (CH_2); 1728, 1706 (carbonyl of NHCOO); 1651 (carbonyl of NHCONH); 1221, 1103 (C-O-C).

^{1}H NMR (DMSO, 400 MHz) δ ppm: 1.24 (s, -CH_2-), 1.49 (m, -CH_2-), 3.13 (s, -$N^+(CH_3)_3$), 3.24 (br, -CH_2-), 3.34 (m, -CH_2OCH_2-), 3.78 (s, Ar-CH_2-Ar), 4.06 (t, -$COOCH_2$), 7.08, 7.34 (m, Ar-H), 9.50 (s, -NHC=O).

2.3.6. Samples preparation

Films used for testing were coated onto a clean glass disk from 10 wt.% polymer in DMF. The solvent was evaporated in an oven at 60 ℃ for 24 h, and the films were further dried in a vacuum oven at 60 ℃ for 48 h. The films were approximately 0.3 mm thick.

2.3.7. Protein adsorption assay.

The adsorption of human fibrinogen onto the films was evaluated using the enzyme-linked immunosorbent assay (ELISA)[21], and the procedures were as described previously[22, 23]. The polyurethane films with 1.0 × 1.0 cm^2 of surface area were incubated with 500 μL of PBS at 37 °C for 60 min, and were then in sequence incubated with 500 μL of 0.5 mg/mL human fibrinogen (Fg, F3879, 55-75% protein, purchased from Sigma, Shanghai) in PBS solution at 37 °C for 120 min, 500 μL of bovine serum albumin (BSA, 2 mg/mL in PBS) solution at 37 ℃ for 90 min, and 500 μL of 5.5 μg/mL horseradish peroxidase (HRP) conjugated Goat anti-human fibrinogen (RCe-0363G, Y-Y Chemical Reagents, Shanghai) in PBS solution at 37 ℃ for 30 min. The polyurethane films were rinsed 5 times with 500 μL of washing buffer and transferred into clean wells, and the enzyme-induced color reaction was then carried by adding 500 μL of 0.1 M citrate-phosphate buffer (pH = 5.0) containing 1 mg/mL chromogen of o-phenylenediamine (OPD) and 0.03% hydrogen peroxide, and finally the absorbance of light intensity at 490 nm was determined by a microplate reader (Model 550, Bio-Rad, USA). The absorbance from the control poly(ether urethane) films is equivalent to 100% for calculating relative adsorption values. Four replicate samples were measured for each concentration in a given experiment. Experiments were done three times.

2.3.8. Platelet adhesion assay

Platelet adhesion measurements were carried out according to the standard protocol as described briefly below. Fresh blood from healthy, drug-free donors was collected using vacuum tubes, containing sodium citrate as an anticoagulant (anticoagulant and blood with the volume ratio of 1:9), and the platelet-rich plasma (PRP) was obtained with the blood centrifuged at 190 g for 10 min. The polyurethane films (10 mm × 10 mm) were placed into a 24-well tissue culture plate and were immersed in 1.0 mL PBS (Phosphate Buffered Saline, pH 7.4) and equilibrated at 37 °C for 1 h. After the PBS was removed, 1.0 mL PRP was poured into each well, and the films were soaked in PRP for 2 h at 37 °C. After the PRP solution was removed, the films were rinsed 3 times with PBS (3 × 1.0 mL), and then treated with 2.5% glutaraldehyde for 1 day at 4 °C. After rinsing with PBS solution, these films were dehydrated with a series of composition gradients of aqueous ethanol solutions (ethanol composition: 0%, 25%, 50%, 75% and 100%). The critical point drying of the specimens was done with liquid CO_2. The dried films were gold coated and then examined with a JEOL Superprobe 733 (JEOL, Japan) scanning electron microscope at 20 kV. Quantitative measurements were made for 5 representative areas of 12 different specimens by image analysis.

2.4. Statistical analysis

All data are expressed as the mean ± standard deviation. One-way ANOVA with Tukey post hoc tests were used for hypothesis testing, with $P < 0.05$ as the measure for statistical significance. The number of independent tests has been listed for each experiment.

3. Results and discussion

3.1. Synthesis of end-capping reagents and polyurethanes

To explore the influence of fluorocarbon chain and phosphorylcholine on the improvement of blood compatibility in polyurethanes, three monomers with

characteristic structure were designed and synthesized, and then were utilized to end-cap polyurethanes. The synthetic routes are shown in Scheme 1 and Scheme 2.

As shown in scheme 1, each of the three end-capping reagents contains an amine ($-NH_2$) as the active functional group to block polyurethane chains, while each of them also has its own distinctive structure. The monomer I ("FA" for short) was based on perfluorooctanoic acid, and the main structure of FA was confirmed through MS and ^{1}H NMR, which are listed in experimental section. The synthesis of monomer II (APPC) was based on 5-amino-1-pentanol, 2-choloro-1,3,2-dioxaphospholane-2-oxide (COP) and trimethylamine according to the Ishihara method[24]. The phosphorylcholine polar head (PC) is the biomimetic functional group. The monomer III (FASPC) was synthesized according to our previous study[22, 23]. In this molecule, the PC head group and long fluorinated tail are both linked to L-serine, and the amine in L-serine is retained as active group. These three monomers decorated with active amine could provide the reaction ability with the isocyanato group of MDI and then endow the polyurethanes with distinctive features.

It is possible to achieve a broad range of properties by varying the hard and soft segment of polyurethanes[25, 26]. In our previous work, the FASPC was introduced to various polyurethanes, and the hemocompatibility of them were all obviously improved without specificity[23]. Then MDI, PTMG and BOD were chosen to synthesize the control polyurethane, which were also the components of some commercial polyurethanes (e.g. pellethane). The stoichiometries of the reaction are shown in Table 1, and the detailed descriptions of synthesis are presented in the experimental section. The control polyurethane and FA, APPC, FASPC end-capped polyurethanes were labeled as PU, PU-F, PU-PC and PU-FPC, respectively.

GPC, ^{1}H NMR, XPS, and element determination were used to confirm the structure and composition of polyurethanes. The weight-average molecular weight (Mw) and number-average molecular weight (Mn) of polyurethanes were determined by GPC (as shown in Table 1), and calibrated based on narrow molecular PMMA standards. It is shown that all their average molecular weights are in the level of 10^4 (between 2.69

$\times 10^4$ and 5.67×10^4 in *M*n). Due to the leaching of unreacted end-cappers and low molecular weight fraction in methanol/distilled water mixed solvent and the nature of solution polymerization, the polydispersities of polyurethanes are all less than 2.0.

The results of ^{1}H NMR are shown in the experimental section. The characteristic peak of phosphorylcholine ($-N^+(CH_3)_3$) in 3.13 ppm appears obviously in both PU-PC and PU-FPC. The characteristic peak of FA does not obviously rise in PU-F due to the small fraction of characteristic hydrogen atoms ($-CF_2-CH_2-$). However, the successful end-capping can be verified by results of XPS and F/P element determinations, the results of which are listed in Table 2. The appearance of F and/or P element in PU-F, PU-PC, and PU-FPC is a direct evidence for the successful end-capping synthesis. The F content in bulk of PU-FPC is lower than that of PU-F, and the same trend is observed in the comparision of P content between PU-FPC and PU-PC, it is assumed that the FASPC monomer has lower reactivity than FA and APPC due to the steric hindrance for amine.

3.2. Structure analysis

As potential biomaterials, both the surface and bulk properties play important roles in the performance of polyurethane materials. Therefore, the surface chemical constitution and the phase separation of polyurethanes were focused on after the introducing of end-cappers.

The XPS date could give direct and on atomic scale chemical information about the surface groups. The atomic concentration of carbon (C_{1s}), oxygen (O_{1s}), nitrogen (N_{1s}), phosphorus (P_{2p}), and fluorine (F_{1s}) in 5-10 nm depth ranged from the surface were detected[23, 27]. The C_{1s} peaks in the four kinds of polyurethanes were fitted to seven component peaks. Among them, the CF_2, CF_3 peaks belong to the fluorinated tail, which rise in the C_{1s} spectra of PU-F and PU-FPC. The C-O-P peak belonged to PC group rises in the C_{1s} spectra of both PU-PC and PU-FPC. However, the C-O-P peak area of PU-FPC is much larger than that of PU-PC, as shown in figure 1a and figure 1c. For composition, the weight contents of F and P in bulk were also detected by element determination method, and the results are also shown in Table 2. The atomic

percentages of F and P on the surface were calculated to weight percentage to adapt to the values in bulk. The wt% of F on the surface of PU-F and PU-FPC are 48.71% and 37.72%. (ignoring the hydrogen fraction), which are 6.3 times and 37.03 times to that in the bulk , the wt% of P in PU-PC and PU-FPC are 2.5 times and 5.8 times on the surface to that in the bulk . The results indicate that the chain ends of polyurethane prossess high mobility and trend to migrate to the surface. However, the end-capping of PC group to polyurethanes chains has limited effect on migration, compared to the easier migration of FA and FASPC groups.

Microphase separation is the main concern for polyurethanes, which play an important role in the surface and bulk properties[28, 29]. In this work, dynamic mechanical analysis (DMA) was employed to study the thermal transitions of polyurethanes, and the change of glass transition temperature (Tg) data of the soft segment phase determined from the peaks of tan δ curves, were used as an indicator of degree of phase separation[29]. The DMA data are shown in Figure 2A, and the Tg data are listed in Table 3. The Tg values of end-capped polyurethanes all decrease than that of control sample, which suggest a trend of enhanced microphase separation in the bulk.

Fluorinated groups are considered as microphase segregating groups, where the perfluoro moiety prefers to be separated from aliphatic and tends to assemble at interface[30-32], therefore, the enhanced microphase separation endows a lower Tg of the soft segment of PU-F than that of the control PU. Zwitterion in block polymer usually plays a role as “binder” between two phases to cause strong microphase separation[33, 34]. Moreover, the steric hindrance of phosphorylcholine group with hard segment and soft segment further strengthens the microphase separation of PU-PC, therefore, the Tg of soft segment of PU-PC is lowest in that of the four kinds of polyurethanes. As for PU-FPC, since the fluorocarbon chain and PC group is linked, the weak intermolecular forces acting on fluorocarbon chains can partly shield the polarizable environment offered by PC group[35], this shield effect inhibits the improvement of microphase separation and performs at a higher Tg compared with that of PU-PC.

In the infrared spectra of polyurethanes, the amide I band ,which is principally due to carbonyl stretching vibration modes, has a relatively well-resolved adsorption doublet, the higher wavenumber peak (about 1730 cm^{-1}) is associated with "free" (non-bonded) C=O stretching adsorption, and the lower wavenumber peak (about 1710 cm^{-1}) mainly represent the adsorption of hydrogen-bonded C=O (with -NH- group) in hard segments[36, 37]. Therefore, the area and wavenumber of H-bonded carbonyl peak can reflect the morphology of hard segment in polyurethanes. The analysis of the FTIR spectra shown in Figure 2B makes use of the above general assignments for the C=O stretching adsorption. To quantitate the examination of the carbonyl starching band, the resolution results of C=O peaks are listed in Table 3[38]. As observed in the FTIR data, upon careful examination of the C=O band, it is evident that the peak area of H-bonded C=O stretching band decreases after end-capping, which indicates the content of hard segment decreases in the bulk of PU-F, PU-PC and PU-FPC; In addition ,all the H-bonded C=O bands of end-capped polyurethanes show a similar trend in shitting to lower wavenumbers, which should be due to the improvement of microphase separation compared to the conventional polyurethane[39, 40].

According to the analysis of infrared spectroscopy and DMA data, the enhanced microphase separation between soft segment and hard segment is proved due to the introducing of fluorinated tail and/or phosphorylcholine group. In addition, the hard segment contents of all the end-capped polyurethane have a trend to decrease in the bulk.

AFM technique was used to further investigate the microphase structure of polyurethane surface in the form of visualization, as shown in Figure 3C. Working at tapping mode, the phase image provides information about surface stiffness variation related to changes in young's modulus, then the microphase-separated structures can be seen in the phase images[29, 41, 42]. The light color regins generally represent hard segment due to the higher modulus.

It should be note that the contrast in phase images is based on the same level of tapping force (amplitudes with range 0.4-0.7). A typical microphase separation pattern

displays on the phase image of the control PU, the hard segment phase size is in dozens of nanometer uniformly. However, the introducing of end-capped changes the surface microdomains of polyurethanes drastically. The fluorocarbon chains of PU-F, which are decorated to hard segment, drive the hard segment to surface due to the low surface energy, and the hard domains almost cover the surface of PU-F[41]. This result is in agreement with XPS data. In the phase image of PU-PC, a decrease in the content of hard domains is observed, while the size of them increase obviously and the boundary between hard domains and soft domains makes sharper than that in the PU phase image. The phase inversion is complete in the PU-FPC phase image. With the aid of fluorinated tail driving, the hard domains enrich on the surface and become the continuous phase, and the soft domains become dispersion phase with "island" shape, as shown in Fig 2C-d. The comparation of surface phase morphology between PU and end-capped polyurethanes in AFM data conforms the similar trend in the enhanced microphase separation behavior for the end-capped polyurethanes in DMA and FTIR analysis. The surface hard segment content of PU-PC are less than that of PU, while the surface hard segment contents of PU-F and PU-FPC are much more than that of PU ,which is reversed to the trend detected in FTIR spectra. It can be deduced obviously that the surface morphologies of end-capped polyurethanes, especially PU-F and PU-FPC, are different from the morphologies in bulk, which is corresponding to the chemical variation from bulk to surface detected by XPS, and the fluorocarbon chains play an important role in this system.

3.3. Surface properties

The time-related water contact angles on the surfaces of the polyurethane films were determined, and the typical figures are shown in Figure 3a. One observes that the water drops on all the polyurethane films show relatively stable contact angles, the drops from momentary angles to equilibrium values in 40 seconds are less than 10^{o}. The high values of water contact angles on PU-F and PU-FPC films (above 115^{o}) should be caused by the appearance of fluorocarbon chains on the top surfaces, which has been verified by XPS data. The angles of PU-PC are slightly less than that of PU

due to the phosphorylcholine groups on the surface. The results indicate that the fluorocarbon chains tend to cover the top surface to minimize the surface free energy after the polyurethane films formed, while the phosphorylcholine groups do not have this trend.

To investigate the rearrangement ability, the polyurethane films were soaked in distilled water at room temperature for one week, and then the water contact angles were determined again after drying under nitrogen, the results of which are shown in Figure 3b. The water contact angle pictures of PU-FPC are also shown for comparison. After the water treatment, all the end-capped polyurethane films have lower water contact angles than the control PU film. This result could be explained by the restructuring of the surface structure [43-45]: after water penetration into the surface and consequent reconstruction of the atoms and molecules at the surface of the substrate, part of the strong hydrophobic fluorocarbon chains migrate to the sub-surface, and the hydrophilic structures, mainly phosphorylcholine groups in this system, tend to migrate to the top surface. The strong mobility of fluorocarbon chains is embodied in this process. However, since the fluorocarbon chain are linked with the phosphorylcholine group on the molecular scale, it should have an effect on the improvement of hydrophility of the whole FASPC moiety for PU-FPC, then it could be understood that the PU-FPC film with more phosphorylcholine groups on the surface but has a higher water contact angle than PU-PC film.

3.4. Hemocompatibility evaluation

Platelet adhesion and activation on the surface of blood-contacting devices will trigger the coagulation of blood, leading to thrombus formation, and protein adsorption is the first step in a cascade of surface processes that induce platelet deposition and thrombus formation. Thus, protein adsorption and platelet adhesion were usually investigated as a preliminary evaluation of the hemocompatibility of materials[46-48], which were also employed in this work.

Fibrinogen (Fg) is one of the most abundant proteins in blood and plays a vital role in thrombosis on material surface, and the adsorption of human fibrinogen on

polyurethane films was detected by ELISA method in this study. This testing method could not obtain the absolute values for Fg adsorbed on film surface in units ($\mu g/cm^2$)[21, 49], so, the Fg adsorption to the control PU film was used as a reference, and the relative Fg adsorptions to end-capped polyurethane films with respect to that on the PU film are shown in Figure 4. In comparison with the control PU, the amount of adsorbed human Fg on PU-F, PU-PC, and PU-FPC decrease by 23.5%, 37.6%, and 78.7%, respectively. Even though the surface of PU-F is covered by fluorocarbon chains, the decrease of adsorbed Fg on PU-F is still less than that of PU-PC, which indicates the phosphorylcholine group are more powerful than fluorocarbon chain for the resistance of protein adsorption. The PU-FPC shows the least amount of Fg adsorption which can be mainly due to the more phosphorylcholine groups. In this preliminary evaluation, Fg adsorption was measured as a single reference to evaluate the protein adsorption. However, It's important to note that other plasma proteins (such as von Willebrands factor, plasminogen or fibronectin) also play important roles in coagulation process[50, 51], which are not tested in this study.

Figure 5 shows the typical SEM photographs of platelet adhesion to polyurethane films. In this study, the blood platelets from multiple donors (three donors) were taken to test, with aim to avoid potential donor-to-donor variations in platelets and their reactivity/adhesion to surfaces[50, 52]. Statistically analyzed by images of parallel samples, the platelet counts on the surfaces of PU, PU-F, and PU-PC are $(1.7 \pm 0.5) \times 10^6$ cm^{-2}, $(4.1 \pm 1.4) \times 10^4$ cm^{-2}, $(2.9 \pm 0.6) \times 10^5$ cm^{-2}, respectively. On the surface of PU-FPC, platelets can hardly be found after the soak for 2 h. There are not only a substantial number of adhered platelets, but also some deformed platelets on the surface of control PU, which indicates that the activation on the adhered platelets may occur. While most of the platelets adhered on PU-F and PU-PC remain a normal shape.

The varying degree of resisting protein adsorption and platelet adhesion by phosphorylcholine groups and fluorocarbon chains in polyurethanes is an interesting phenomenon in this study. It has been known that both fluorocarbon chain and PC group on polymer surface can prevent protein adsorption and platelet adhesion to

improve blood compatibility[12, 20, 53], the experimental data in this study also verify this trend, while the degree of improvement in each aspect is different. In protein adsorption study, the amount of PC groups present at surface of PU-PC is much less than that of fluorocarbon chains at PU-F surface (XPS and AFM data), but the fibrinogens adsorbed on PU-PC are still less than that on PU-F, which obviously indicates more efficiency of PC group in preventing proteins. The contrary trend is found in the platelet adhesion experiment. The amount of platelets adhered to PU-F is one order smaller than that adhered to PU-PC, which means the fluorocarbon chains in PU-F reduce the adhesion of platelets more efficiently than PC groups in PU-PC. It can conclude that, in polyurethanes, the fluorocarbon chains are more efficient for resisting platelet adhesion, while the PC groups prevent fibrinogen adsorption effectively. Moreover, when fluorocarbon chain and PC group are simultaneously introduced to polyurethane, the hemocompatibility (in both protein adsorption and platelet adhesion experiments) is improved dramatically in this preliminary study. This synergistic effect triggered by two anticoagulation components in polyurethane is promising, and is worthy for quantitative research in detail and in other materials in the future.

4. Conclusions

In this work, three monomers containing fluorinated tail and/or phosphorylcholine for end-capping were synthesized and introduced to polyurethanes. It is found that the fluorocarbon chains and phosphorylcholine groups can have synergistic effect on the improvement of hemocompatibility in polyurethanes, and the advanced properties are mainly due to these reasons:

1. The migration ability of fluorocarbon chains can drive the phosphorylcholine groups to enrich on the surface of polyurethane films.
2. The spontaneous arrangement of fluorocarbon chains and phosphorylcholine groups makes them have a balance on the surface to adapt to the water environment.

3. Both fluorocarbon chain and phosphorylcholine group in polyurethanes have their own advantages on anticoagulation, and each of them can play a vital role in the progress of clotting cascade.

Although the synergistic effect of fluorocarbon chain and phosphorylcholine group on anticoagulation still need to be further clarified in detail and in vivo, the results of this work indicate that the combination of anticoagulation components in the same material has real potential to develop biomaterials contacting with blood.

Acknowledgments

This work is a collaborative research project sponsored by the Ministry of Science and Technology of China (grant no. 2010DFA31190) and the Government of Quebec, Quebec, Canada (grant no. PSR-SIIRI-285). We would also like to express our sincere thanks to the National Natural Science Foundation of China for Financial Support (51121001).

Notes and References

1. H. S. Lee, N. Tomczyk, J. Kandel, R. J. Composto and D. M. Eckmann, *J. Mater. Chem. B.*, 2013, **1**, 6382-6391.
2. F. Tong, X. Chen, L. Chen, P. Zhu, J. Luan, C. Mao, J. Bao and J. Shen, *J. Mater. Chem. B.*, 2013, **1**, 447-453.
3. R. Y. Kannan, H. J. Salacinski, P. E. Butler, G. Hamilton and A. M. Seifalian, *J. Biomed. Mater. Res. B.*, 2005, **74B**, 570-581.
4. K. Kashimoto, J. Yoon, B. Y. Hou, C. H. Chen, B. H. Lin, M. Aratono, T. Takiue and M. L. Schlossman, *Phy. Rev. Lett.*, 2008, **101**, 076102.
5. I. Lee, K. Kobayashi, H. Y. Sun, S. Takatani and L. G. Zhong, *J. Biomed. Mater. Res. A.*, 2007, **82A**, 316-322.
6. H. Yin, T. Akasaki, T. L. Sun, T. Nakajima, T. Kurokawa, T. Nonoyama, T. Taira, Y. Saruwatari and J. P. Gong, *J. Mater. Chem. B.*, 2013, **1**, 3685-3693.
7. A. P. Khandwekar, D. P. Patil, A. A. Hardikar, Y. S. Shouche and M. Doble, *J.Biomed. Mater. Res. A.*, 2010, **95A**, 413-423.
8. R. Leitsmann, O. Bohm, P. Planitz, C. Radehaus, M. Schaller and M. Schreiber, *Surf. Sci.*, 2010, **604**, 1808-1812.
9. X. Y. Xie, R. F. Wang, J. H. Li, L. Luo, D. Wen, Y. P. Zhong and C. S. Zhao, *J. Biomed. Mater. Res. B.*, 2009, **89B**, 223-241.
10. T. Hong, X. Xingyi, L. Jiehua, Z. Yingping and F. Qiang, *Polymer*, 2004, **45**, 1495-1502.

11. G. Jiang, X. Tuo, D. Wang and Q. Li, *J. Mater. Sci.-Mater. M.*, 2012, **23**, 1867-1877.
12. K. Y. Chen and J. F. Kuo, *J. Mater. Sci.-Mater. M.*, 2002, **13**, 37-45.
13. J. C. Lin, S. L. Tiong and C. Y. Chen, *J. Biomat. Sci-Polym. E.*, 2000, **11**, 701-714.
14. H. Wang, F. Xu, Y. Wang, X. Liu, Q. Jin and J. Ji, *Polym. Chem.*, 2013, **4**, 3012-3019.
15. P. Wan, D. Tan, Z. Li, X. Zhang, J. Li and H. Tan, *Chinese. J. Polym. Sci.*, 2012, **30**, 190-198.
16. T. Goda, H. Furukawa, J. P. Gong and K. Ishihara, *Soft. Matter.*, 2013, **9**, 2166-2171.
17. M. Tan, Y. Feng, H. Wang, L. Zhang, M. Khan, J. Guo, Q. Chen and J. Liu, *Macromol. Res.*, 2013, **21**, 541-549.
18. T. Hatakeyama, M. Tanaka and H. Hatakeyama, *Acta. Biomater.*, 2010, **6**, 2077-2082.
19. K. Ishihara, H. Nomura, T. Mihara, K. Kurita, Y. Iwasaki and N. Nakabayashi, *J. Biomed. Mater. Res.*, 1998, **39**, 323-330.
20. Y. Iwasaki, Y. Aiba, N. Morimoto, N. Nakabayashi and K. Ishihara, *J. Biomed. Mater. Res.*, 2000, **52**, 701-708.
21. Z. Zhang, T. Chao, S. F. Chen and S. Y. Jiang, *Langmuir*, 2006, **22**, 10072-10077.
22. D. Tan, X. Zhang, J. Li, H. Tan and Q. Fu, *J. Biomed. Mater. Res. A.*, 2012, **100A**, 380-387.
23. X. Zhang, D. Tan, J. Li, H. Tan and Q. Fu, *Biofouling*, 2011, **27**, 1175-1175.
24. K. Ishihara, T. Uchida and N. Nakabayashi, *Polym. J.,* 1990, **22**, 355-360.
25. Y. W. Tang, R. S. Labow and J. P. Santerre, *J. Biomed. Mater. Res.*, 2001, **56**, 516-528.
26. T. Choi, J. Weksler, A. Padsalgikar and J. Runt, *Polymer*, 2009, **50**, 2320-2327.
27. J. Tan and J. L. Brash, *J. Appl. Polym. Sci.*, 2008, **108**, 1617-1628.
28. L. C. Xu, J. Runt and C. A. Siedlecki, *Acta. Biomater.*, 2010, **6**, 1938-1947.
29. H. Tan, J. H. Li, M. Guo, R. N. Du, X. Y. Xie, Y. P. Zhong and Q. Fu, *Polymer*, 2005, **46**, 7230-7239.
30. S. J. Cowling, A. W. Hall and J. W. Goodby, *J. Mater. Chem. ,* 2011, **21**, 9031-9042.
31. G. De Luca, A. Liscio, M. Melucci, T. Schnitzler, W. Pisula, C. G. Clark, Jr., L. M. Scolaro, V. Palermo, K. Muellen and P. Samori, *J. Mater. Chem.*, 2010, **20**, 71-82.
32. Y. Zhang, L. Wang, Z. Zhang, Y. Zhang and X. Tuo, *J. Polym. Sci. Polym. Chem.*, 2013, **51**, 2161-2170.
33. E. Marwanta, T. Mizumo and H. Ohno, *Solid. State. Ionics.*, 2007, **178**, 227-232.
34. S. Pispas, G. Floudas and N. Hadjichristidis, *Macromolecules*, 1999, **32**, 9074-9077.
35. X. Wang, P. Long, S. Dong and J. Hao, *Langmuir*, 2013, **29**, 14380-14385.
36. M. M. Coleman, D. J. Skrovanek, J. Hu and P. C. Painter, *Macromoleculars*, 1988, **21**, 59-68.
37. D. Tan, X. Zhang, J. Li, H. Tan and Q. Fu, *Appl. Surf. Sci.*, 2012, **258**, 2697-2706.
38. D. Tan, X. Zhang, J. Li, H. Tan and Q. Fu, *Chinese. J. Polym. Sci.*, 2011, **29**, 615-626.
39. D. A. Wang, J. Ji and L. X. Feng, *Macromolecules*, 2000, **33**, 8472-8478.
40. G. Trovati, E. Ap Sanches, S. C. Neto, Y. P. Mascarenhas and G. O. Chierice, *J. Appl. Polym. Sci.*, 2010, **115**, 263-268.
41. M. Penoff, W. Schreiner, P. Oyanguren and P. Montemartini, *Macromol. Symp.* 2012, **321-322**, 186-190.
42. Y. Yanagihara, N. Osaka, S. Murayama and H. Saito, *Polymer*, 2013, **54**, 2183-2189.
43. X. Cui, S. Zhong, Y. Gao and H. Wang, *Colloid. Surface. A.*, 2008, **324**, 14-21.
44. S. Perutz, J. Wang, E. J. Kramer, C. K. Ober and K. Ellis, *Macromolecules*, 1998, **31**, 4272-4276.

45. D. L. Schmidt, R. F. Brady, K. Lam, D. C. Schmidt and M. K. Chaudhury, *Langmuir*, 2004, **20**, 2830-2836.
46. H. W. Chien, C. C. Tsai, W. B. Tsai, M. J. Wang, W. H. Kuo, T. C. Wei and S. T. Huang, *Colloid. Surface. B.*, 2013, **107**, 152-159.
47. J. Tan, W. G. McClung and J. L. Brash, *J. Biomat. Sci.-Polym. E.*, 2013, **24**, 497-506.
48. L. Ma, H. Qin, C. Cheng, Y. Xia, C. He, C. Nie, L. Wang and C. Zhao, *J. Mater. Chem. B.*, 2013. DOI: 10.1039/C3TB21388A.
49. J. Li, Y. Zhang, J. Yang, H. Tan, J. Li and Q. Fu, *J. Biomed. Mater. Res. A.*, 2013, **101A**, 1362-1372.
50. M. Zhang and T. A. Horbett, *J. Biomed. Mater. Res. A.*, 2009, **89A**, 791-803.
51. L. M. Szott and T. A. Horbett, *Curr. Opin. Chem. Biol.*, 2011, **15**, 677-682.
52. J. M. Grunkemeier, W. B. Tsai and T. A. Horbett, *J. Biomed. Mater. Res.*, 1998, **41**, 657-670.
53. M. Pagliaro and R. Ciriminna, *J. Mater. Chem.*, 2005, **15**, 4981-4991.

Table and Figure captions

Table 1. Stoichiometry, molecular weights and yield of the polyurethanes

Samples	Stoichiometry	Molecular weight*			Yield (%)
	MDI:PTMG:BDO:end-capper	Mn $\times 10^{-4}$	Mw $\times 10^{-4}$	Mw/Mn	
PU	3:2:1:0	5.67	8.53	1.50	78
PU-F	3:2:0.5:1	2.75	4.87	1.77	71
PU-PC	3:2:0.5:1	2.69	4.64	1.72	82
PU-FPC	3:2:0.5:1	3.50	5.68	1.62	75

* Gel permeation chromatography (GPC) was performed by Waters-1515 using N, N-dimethylformamide (DMF)/LiBr as eluent. The molecular weights are relative to polymethyl methacrylate (PMMA) standards.

Table 2. Element contents of polyurethanes on the surface and in the bulk.

Samples	Element contents on the surface (at.%) [a]					Element contents in the bulk (wt.%) [b]	
	C	O	N	P	F	P	F
PU	76.27	21.90	1.83	0	0	—	—
PU-F	48.81	7.65	4.79	0	38.75	0	7.67 ± 0.26
PU-PC	77.48	19.73	2.50	0.29	0	0.28 ± 0.02	0
PU-FPC	51.94	12.07	6.16	0.53	29.30	0.19 ± 0.06	1.02 ± 0.01

[a] Values detected by XPS; [b] values detected by element determination ; "—" without detection.

Table 3. Glass transition temperatures detected by DMA and the C=O stretching band information of polyurethanes

Samples	Tg of soft segment (^{o}C)	"free" C=O		H-bonded C=O	
		Stretching band υ(cm^{-1})	Area percentage (%)	Stretching band υ(cm^{-1})	Area percentage (%)
PU	-17.05	1729	37.8	1707	62.2
PU-F	-18.88	1729	39.7	1706	60.3
PU-PC	-24.31	1730	40.4	1704	59.6
PU-FPC	-18.33	1730	38.7	1702	61.3

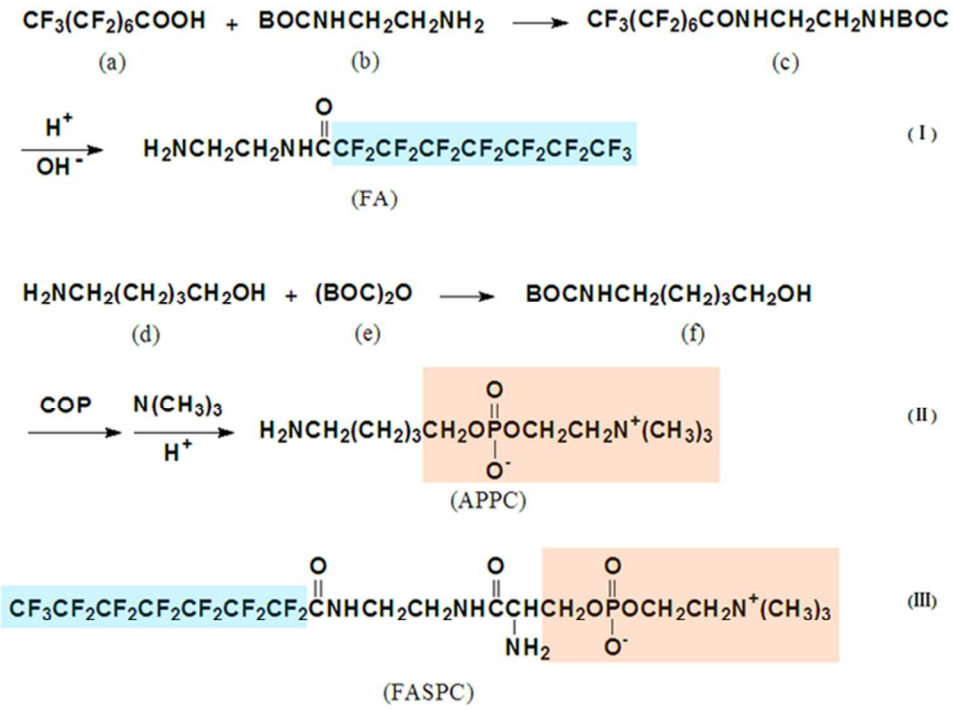

The synthesis routes and structures of monomers
59x44mm (300 x 300 DPI)

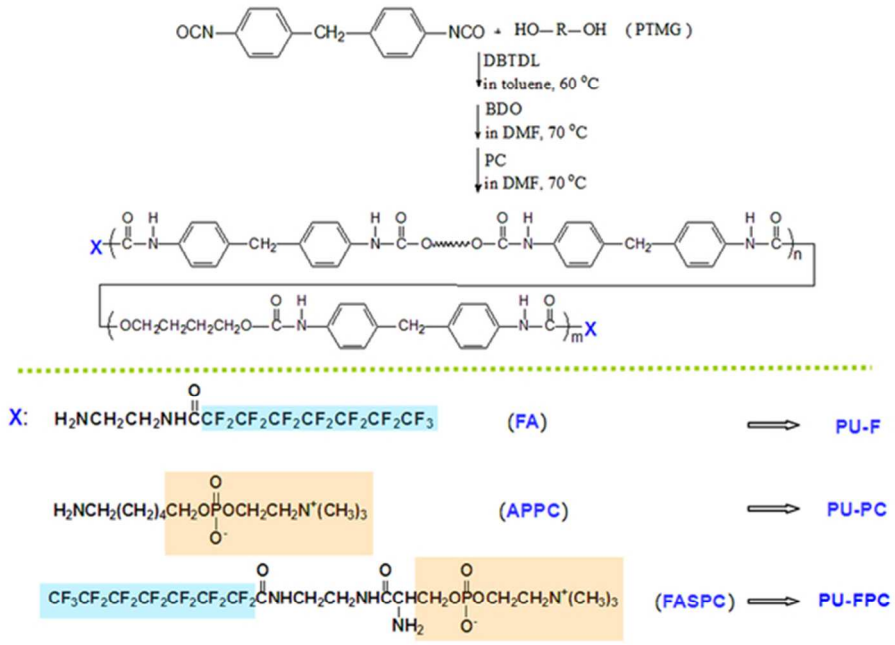

The synthesis of polyurethanes end-capped with monomers
57x41mm (300 x 300 DPI)

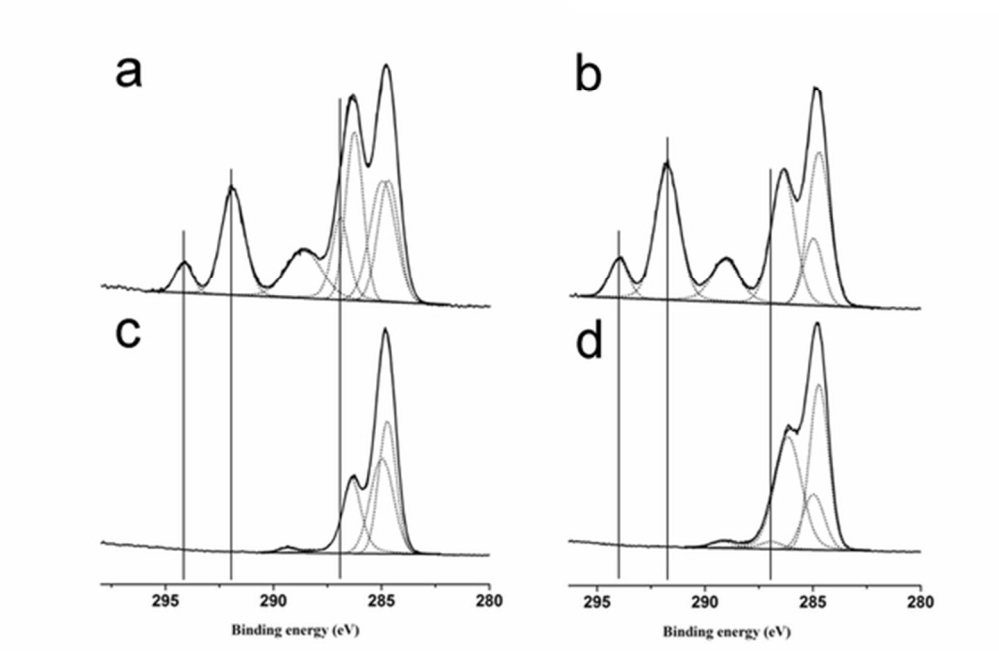

XPS spectra of carbon (C1s) of PU-FPC (a), PU-F (b), control PU (c), and PU-PC (d)
52x34mm (300 x 300 DPI)

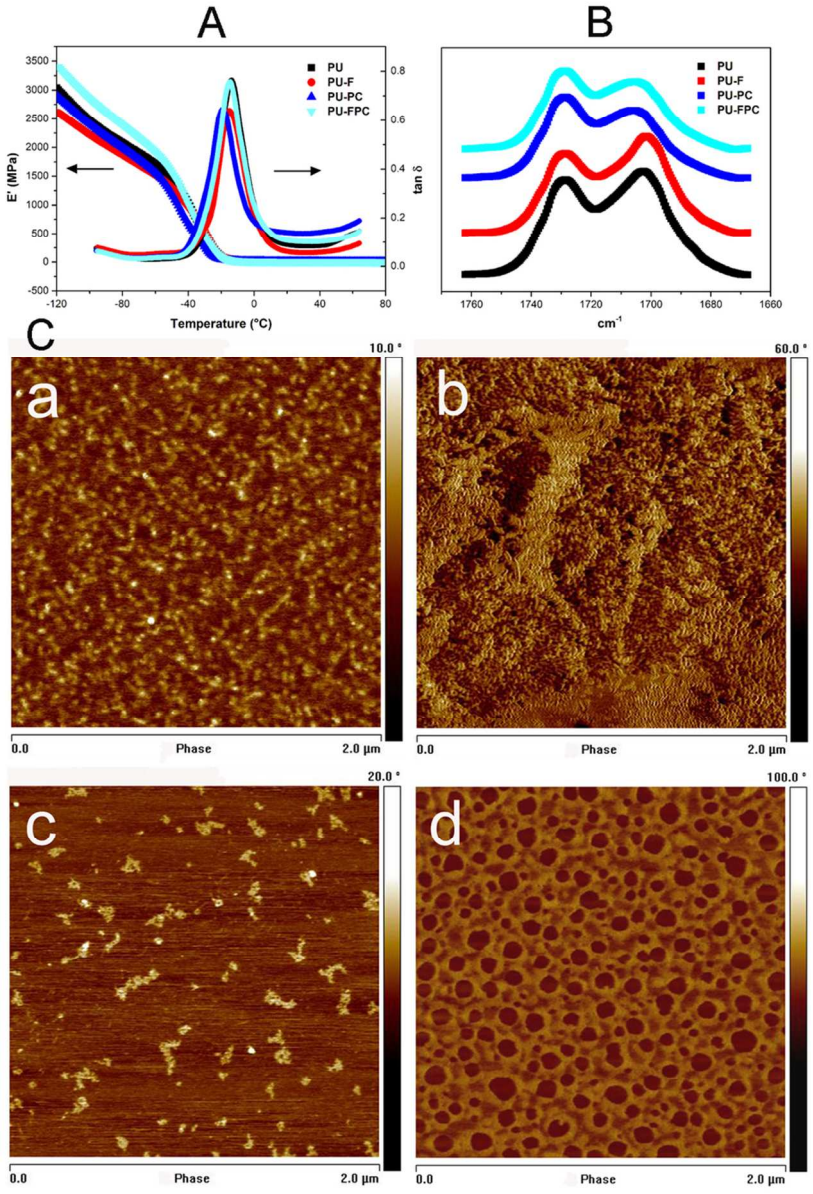

A. dynamic-mechanical spectrum of polyurethanes; B. C=O stretching band in FTIR spectra of polyurethanes; C. AFM phase images of control PU (a), PU-F (b), PU-PC (c), and PU-FPC (d).
80x118mm (300 x 300 DPI)

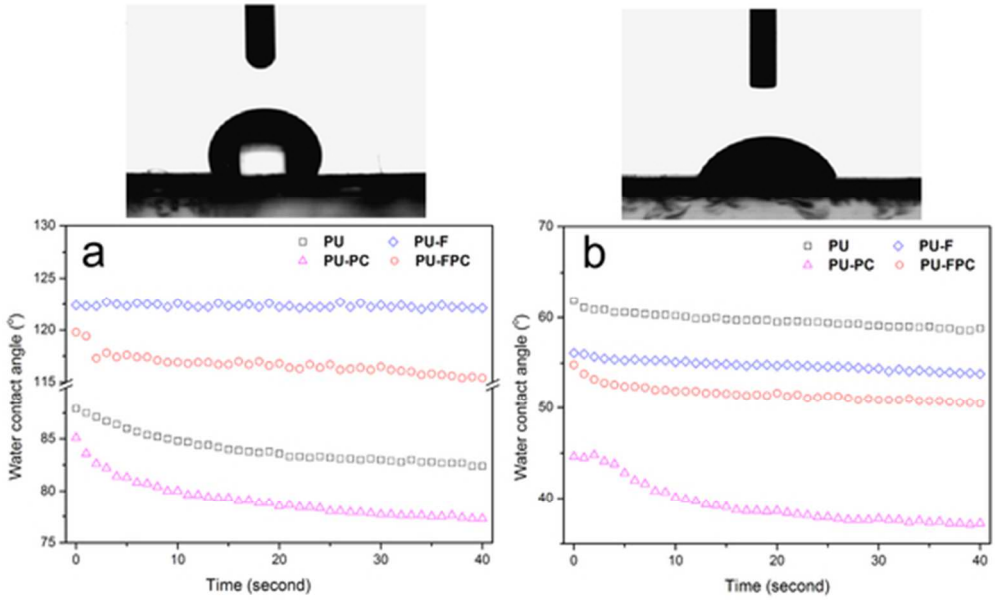

The water contact angles of polyurethanes before (a) and after (b) water treatment for one week. The water contact angle pictures belong to PU-FPC.
48x29mm (300 x 300 DPI)

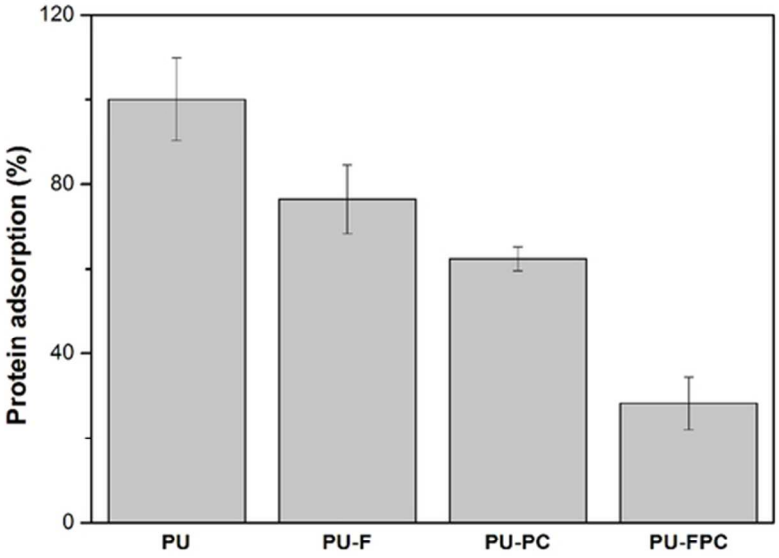

Relative human fibrinogen adsorption on various polyurethanes determined from ELISA with control PU as a reference. *Statistically significant difference with respect to control PU ($p < 0.05$).
56x39mm (300 x 300 DPI)

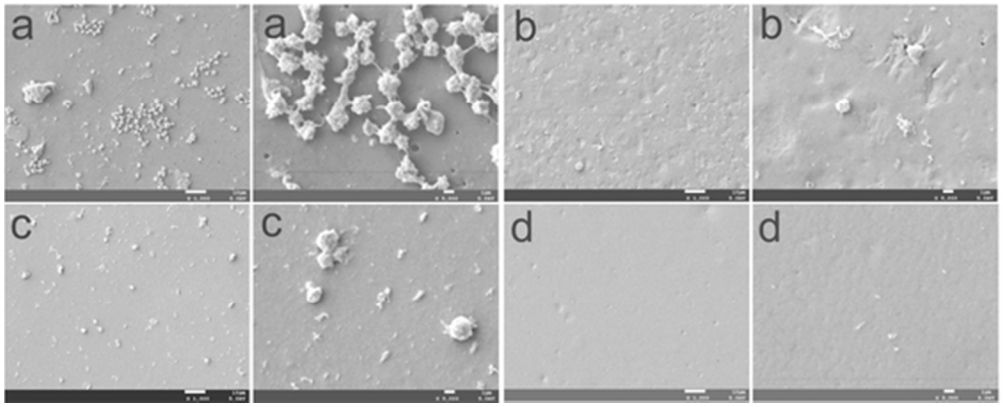

SEM images of the surface of polyurethane films after 2 h of PRP exposure. (a) PU; (b) PU-F; (c) PU-PC; (d) PU-FPC. Actual magnification: left 1000 ×; right 5000 ×.
47x19mm (300 x 300 DPI)